Electrochimica Acta 156 (2015) 154–162

Contents lists available at ScienceDirect

Electrochimica Acta

journal homepage: www.elsevier.com/locate/electacta

Spectroelectrochemical study of picolinic acid adsorption during silver electrodeposition

Cecilia I. Vázquez [a,*], Gustavo F.S. Andrade [c], Marcia L.A. Temperini [b], Gabriela I. Lacconi [a,*,1]

[a] INFIQC CONICET, Dpto. de Fisicoquímica, Facultad de Ciencias Químicas, Universidad Nacional de Córdoba, Ciudad Universitaria, RA-5000 Córdoba, Argentina
[b] Laboratório de Espectroscopia Molecular, Instituto de Química, Universidade de São Paulo, C.P. 26077, CEP 05.513–970, São Paulo, Brazil
[c] Departamento de Química, Instituto de Ciências Exatas, Universidade Federal de Juiz de Fora, Martelos, CEP 36036–900, Juiz de Fora, Brazil

ARTICLE INFO

Article history:
Received 6 October 2014
Received in revised form 31 December 2014
Accepted 9 January 2015
Available online 12 January 2015

Keywords:
Surface-Enhanced Raman Spectroscopy
silver electrodeposition
picolinic acid
adsorption

ABSTRACT

The adsorption of picolinic acid (PA) onto HOPG electrodes during silver electrodeposition at pH 3.0 was examined using conventional electrochemical techniques: cyclic voltammetry and impedance measurements (differential capacity-potential plots) and Surface-Enhanced Raman Spectroscopy (SERS), through a wide range of electrode potentials. The spectroelectrochemical results indicate that the electroactive species for silver electrodeposition are Ag^+ ions and [Ag(Pic)] complexes, in spite of the predominant species in solution being the zwitterion (HPic). Adsorption of the anion (Pic^-) occurs through a wide potential range where the electrode surface charge density is positive. However, HPic deprotonation, hydrogen formation and Pic^- desorption, with the consequent decrease in SERS intensity, occur at the zero-charge potential (pzc) for HOPG.

1. Introduction

Metal electrodeposition stands out between the most significant applications of electrochemistry as a technique that enables the deposition of a wide variety of nanostructures onto conductor and semiconductor substrates at ambient temperature. The quality of the deposits depends on experimental conditions such as electrode potential, current density, surface pretreatment, electrolyte composition, and the presence of organic additives in the bath [1,2]. Adsorption of molecules with different functional groups at the deposited metal surface influences for example, the nucleation rate, thereby resulting in different deposit morphologies, surface distribution on the surface, and properties at the nanoscale [3–6].

Obtaining information about the electrode/electrolyte interface during the electrodeposition process is very important for both technological applications and fundamental research. Surface-Enhanced Raman Spectroscopy (SERS) has been extensively used to study different processes through identification of various organic addition agents and corrosion inhibitors [7,8]. Detection and identification of adsorbates are feasible when a SERS-active substrate is available. However, a quantitative analysis of the surface concentration is not easy because the orientation of the adsorbed molecules is related to the selection rules for active Raman vibrational modes and the dependence of surface coverage on electrode potential. An approach based on combining Raman spectroscopy and electrochemical techniques, such as cyclic voltammetry and impedance measurements, can provide information concerning direct adsorbate interactions at metal/electrolyte interface during the electrodeposition process [9].

In this work, we investigate silver deposition onto HOPG electrodes with picolinic acid (PA) as an additive in the electrolyte. Use of this organic molecule as a non-toxic addition agent in metal electrodeposition is of particular interest, because of its tendency to coordinate with metal ions and its ability to be adsorbed onto different surfaces via carboxylate and pyridinic-nitrogen functional groups [10,11]. In a recent investigation of PA-influenced copper electrodeposition on vitreous carbon, Bolzán found two cathodic contributions which were assigned to the electroreduction of copper ions and $[Cu(PA)_2]^{2+}$ soluble complex species [12]. Our own investigations have examined the influence of pyridine-carboxylic acids on nucleation and growth mechanism in silver and copper electrodeposition, and have shown that PA species can be strongly

* Corresponding authors. Tel.: +54 351 5353866; fax: +54 351 4334188.
E-mail addresses: cecizqz@gmail.com (C.I. Vázquez), Gabriela.Lacconi@gmail.com, glacconi@mail.fcq.unc.edu.ar (G.I. Lacconi).
[1] ISE member.

http://dx.doi.org/10.1016/j.electacta.2015.01.034
0013-4686/

adsorbed on the growing nuclei surface, thereby inhibiting its reactivity and providing a mechanism for dendritic growth [10,13]. In addition, we have also explored the influence of solution pH on voltammetric response, SERS spectra, and silver crystallites morphology, and we have found that the PA anion species is adsorbed at pH values higher than 3.0, while adsorption of both anion and zwitterion species occurs at a pH value of 0.3 [14].

Since the mechanism of silver electrodeposition onto HOPG in the presence of PA is already known [13,14], the focus of the present study lies on investigate the adsorption process of additive molecules on growing crystallites over a wide range potential, in solutions of pH 3.0. SERS spectroscopy with potentiodynamic control of the electrode/solution interface has been shown to be a powerful tool for the sensitive detection of different species of PA on the electrode surface. In addition, differential capacity behavior exhibits strong correlations with spectroelectrochemical experiments.

2. Experimental Section

2.1. Chemicals

All electrolytic solutions used in this work were freshly prepared with analytical grade reagents, without further purification and ultrapure water from a Millipore-Milli-Q system with 18.2 MΩ·cm resistivity. Chemical reagents were silver perchlorate (BDH Chemicals Ltd. 98%), picolinic acid (Sigma-Aldrich, 99%) and potassium perchlorate (J.T. Baker). All solutions were degassed with N_2 for 20 minutes before use, and the pH was adjusted by addition of perchloric acid.

2.2. Electrochemical procedures

Electrochemical measurements were carried out at room temperature in a conventional three-electrode glass cell. Highly oriented pyrolytic graphite (HOPG SPI Supplies, Brand Grade SPI-1, $10 \times 10\,mm^2$) in a Teflon holder with an exposed circular region of $0.283\,cm^2$ was used as working electrode. The basal plane surface of HOPG crystal was cleaved using adhesive tape immediately prior to use. A Pt wire was the counter electrode and a silver wire immersed in the electrolyte was the quasi-reference electrode. All potentials are reported vs. Ag/Ag^+ (1.0 mM) reference electrode (E_{Ag/Ag^+} = -0.30 V vs. SCE).

Prior to each electrochemical experiment, a reproducible state of the HOPG surface was attained by polarization of the electrode at 0.4 V for about 3 min [15,16]. Cyclic voltammetry was performed by scanning from 0.4 V towards negative potentials with an Autolab (PGSTAT ECO CHEMIE) electrochemical workstation. Electrochemical impedance spectroscopy (EIS) measurements were acquired with a Solartron 1260 electrochemical interface in the 10^{-1} to 10^5 Hz frequency range with 0.01 V signal amplitude. The differential capacity experiments were recorded at 20 Hz with a scan rate of $10\,mV\,s^{-1}$. Capacity-potential curves were obtained by fitting the ac impedance measurements with a simple RC equivalent circuit representing the electric double layer model.

2.3. SERS experiments

Spectroelectrochemical SERS measurements were performed with a Renishaw InVia microRaman spectrometer, equipped with a Leica microscope and 63x water immersion objective (NA = 0.9). The 632.8 nm line of a He-Ne Coherent 31-2140-000 laser with a power of 3.5 mW and $1.0\,\mu m^2$ illuminated area on the sample was used. In-situ SERS measurements were carried out in a homemade-Teflon cell with the HOPG electrode in the bottom (exposed area was $0.40\,cm^2$), a Pt wire loop as counter electrode, and Ag/Ag^+ quasi-reference electrode. The spectra were obtained during a potentiodynamic scan at a rate of $1\,mV\,s^{-1}$; with the acquisition mode consisting of 10 s accumulation at each point during the scanning process and resulting in a scan time of ca. 60 s for spectrum. The electrochemical potential in the SERS experiments was applied with a potentiostat/galvanostat EG&G PAR-273 interfaced to a computer. The reported potential values were taken at the end of each SERS spectrum.

2.4. Morphological characterization

Scanning electron microscopy (SEM) images were taken with a JEOL Field Emission Gun model JSM-7401F, with an acceleration voltage of 5 kV and a filament current of 10 μA.

3. Results and Discussion

3.1. Silver electrodeposition onto HOPG in the presence of PA

Picolinic acid (2-pyridine carboxylic acid) has two functional groups, the carboxylic group in the α-position and the pyridinic-nitrogen site, whose acid equilibrium constants are $pKa_1 = 1.03$ and $pKa_2 = 5.21$, respectively [17]. The predominant chemical species in aqueous-PA solution are $\mathbf{H_2Pic^+}$ (protonated) at pH < 1.03, **HPic** (zwitterion) at pH around 3.0, and $\mathbf{Pic^-}$ (anion) at pH > 5.21. From a chemical structure viewpoint, only the latter two species have functional groups available for coordination with silver ions present in the electrolytic solution. The stability constants for the corresponding 1:1 complexes are given by reactions (1) and (2) at pH 3.0 and 6.5, respectively [13,14].

$$Ag^+ + HPic \rightleftarrows [Ag(HPic)]^+ \quad K_{[Ag(HPic)]^+} = (11.5 \pm 0.6)\,M^{-1} \tag{1}$$

$$Ag^+ + Pic^- \rightleftarrows [Ag(Pic)] \quad K_{[Ag(Pic)]} = (800 \pm 100)\,M^{-1} \tag{2}$$

In order to study the effect of PA during silver electrodeposition onto and stripping from HOPG, j/E potentiodynamic profiles were obtained in both presence and absence of 0.5 mM PA in 0.1 M $KClO_4$ and 1.0 mM $AgClO_4$ solution at pH 3.0, with the predominant additive species under these conditions being **HPic**. In the cathodic scan of the first potentiodynamic cycle recorded in 0.5 mM PA solution (Fig. 1), the onset potential for silver deposition is -0.15 V

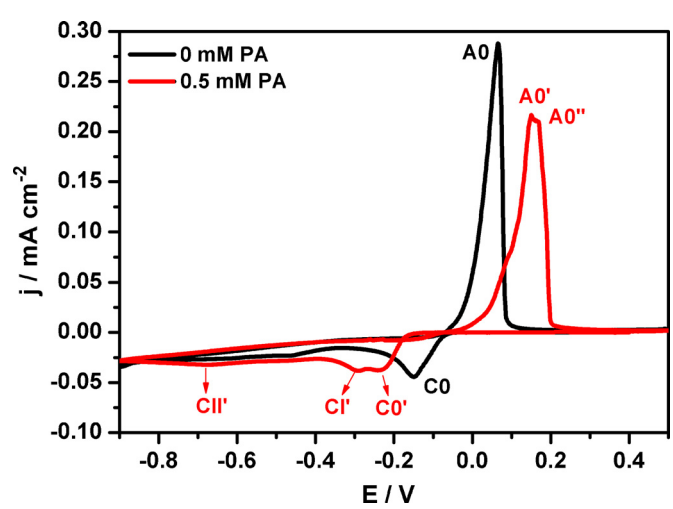

Fig. 1. Potentiodynamic j/E profiles of silver deposition onto HOPG in 0.1 M $KClO_4$ + 1.0 mM $AgClO_4$ solutions at pH 3.0, in the absence (black line) and presence of 0.5 mM PA (red line). Scan rate: $1\,mV\,s^{-1}$. (For interpretation of the references to colour in this figure legend, the reader is referred to the web version of this article.)

and a current density maximum with two components, **C0'** (at -0.24 V) and **CI'** (at -0.29 V), is observed. Furthermore, another cathodic peak labeled **CII'** is apparent at -0.7 V, and its origin is discussed in Section 3.3. Upon reversing the potential scan, two anodic contributions (**A0'** and **A0"**) associated with silver dissolution are observed at potentials more positive than those in the additive-free electrolyte.

Shifting of silver deposition to more negative potentials and decrease of the voltammetric charge are the main effects of increasing the additive content in solution. In addition, the position of the **C0'** peak is found to be affected by PA concentration and solution pH, as shown in Fig. 2.

In previous reports, PA has been shown to act as an inhibitor of metal deposition processes onto different substrates, due to solution metal-ion complexation and surface adsorption [10,13]. In the present case, the cathodic current peaks can be assigned to the electroreduction of Ag^+ ions and **[Ag(PA)]** species, according to the following reactions [13,14]:

C0' peak:

$$Ag^+ + e^- \overset{k_3}{\rightarrow} Ag^0 \quad (3)$$

CI'peak:

$$[Ag(Pic)] + e^- \overset{k_4}{\rightarrow} Ag^0 + Pic^- \quad (4)$$

The reduction process corresponding to the **C0'** peak is slightly shifted from the **C0** peak potential because of additive adsorption onto the electrode surface, and can be associated with Ag^+ ions electroreduction (Eq. (3)).

It has been mentioned that the predominant PA species in solution at pH 3.0 is the zwitterion (**HPic**), which can form soluble 1:1 complexes with Ag^+ ions according to Eq. (2). However, for analytical concentrations of 0.5 mM PA and 1.0 mM Ag^+, the equilibrium concentration of **[Ag(HPic)]$^+$** is 0.006 mM and 0.011 mM, respectively, and therefore practically all the Ag^+ ions are not complexed, as shown in Table 1. This is undoubtedly due to the very low value of $K_{[Ag(HPic)]^+}$ (Eq. (1)). Hence, the **CI'** peak cannot be assigned to the **[Ag(HPic)]$^+$** reduction. This cathodic process occurs at almost the same potential as the electroreduction of **[Ag(Pic)]** complexes at pH 6.5, which does not depend on the PA concentration (results not shown). Nevertheless, in-situ SERS spectra recorded in this potential range (Section 3.2) show that the additive species present at the interface is **Pic$^-$**, providing molecular-level evidence for the reduction reaction of **[Ag(Pic)]** complexes associated with the **CI'** peak (Eq. (4)) [13,14].

Table 1
Concentrations at equilibrium of species present in 1.0 mM $AgClO_4$ solutions with different PA concentrations at pH 3.0.

PA anal. concentr. /mM	Equilibrium concentrations at pH 3.0/mM					
	Ag^+	H_2Pic^+	*HPic*	*Pic*$^-$	[Ag(*HPic*)]$^+$	[Ag(*Pic*)]
0.5	0.992	0.005	0.484	0.003	0.006	0.002
1.0	0.984	0.010	0.968	0.006	0.011	0.005
5.0	0.926	0.052	4.844	0.030	0.052	0.022

Values calculated considering the acid dissociation and the complexes stability (Reactions (1) and (2)) constants.

Regarding the anodic peaks **A0'** and **A0"**, as the current maxima for silver deposition from **[Ag(Pic)]** complexes (**CI'**) was found at more negative potentials relative to silver deposition from Ag^+ ions (**C0'**), the anodic contribution **A0"** cannot be assigned to silver dissolution to **[Ag(Pic)]**, which should be found at lower potentials than **A0**. During silver dissolution (at potentials higher than -0.07 V) there is a high increase in Ag^+ ions concentration at the electrode/electrolyte interface containing PA adsorbed, which facilitates the formation of an insoluble surface complex Ag-PA that blocks the dissolution of remaining silver deposit. Thus, this deposit can only be electrodissolved at more positive potentials. This effect is more pronounced at higher potential scan rates, as it was shown in [13], where a noticeable separation between the potentials of **A0'** and **A0"** peaks is observed. This result is further confirmed by spectroelectrochemical experiments, since SERS intensity of vibrational signals for **Pic$^-$** continues to be observed even at potentials more positive than those of silver anodic dissolution (see Section 3.2).

3.2. In situ SERS measurements during silver electrodeposition onto HOPG in the presence of PA

In order to confirm the assignment of voltammetric peaks, we have carried out spectroelectrochemical experiments, by recording the SERS signals from the adsorbed species during

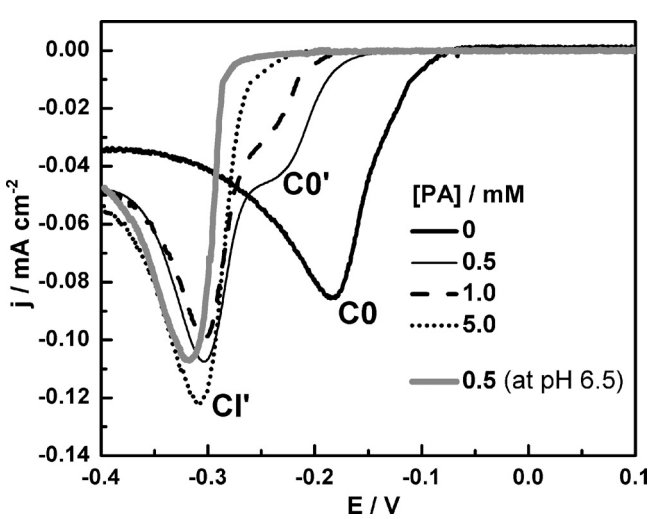

Fig. 2. Potentiodynamic j/E profiles of silver deposition onto HOPG in 0.1 M $KClO_4$ + 1.0 mM $AgClO_4$ + x mM PA ($0 \leq x \leq 5$) solutions at pH 3.0 and 6.5. Scan rate: 5 mV s^{-1}.

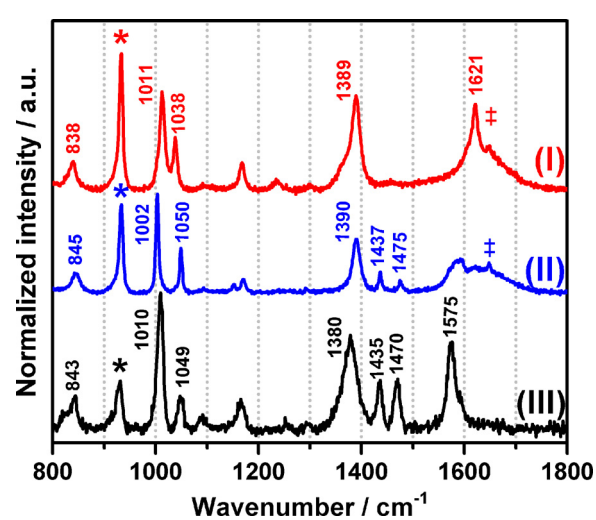

Fig. 3. Normal Raman spectra of PA (0.15 M) in 0.1 M $KClO_4$ at (I) pH 3.0 and (II) pH 6.5 aqueous solutions. (III) In-situ SERS spectrum during the potentiodynamic silver deposition onto HOPG in 0.1 M $KClO_4$ + 1.0 mM $AgClO_4$ + 0.5 mM PA at pH 3.0 performed to -0.45 V at 1 mV s^{-1}. (*) Raman band from ClO_4^- ions. (‡) Signal at **1648** cm^{-1} from the 632.8 nm laser plasma.

Table 2
Vibrational assignments of the main bands in the PA spectra from Fig. 3, which were obtained from DFT calculations and bibliography [14,18,19].

Wavenumber/cm^{-1}			Assignment[a]
Normal Raman			
		SERS at -0.45 V	
pH 3.0 *HPic* (I)	pH 6.5 *Pic*$^-$ (II)	pH 3.0 (III)	
838			ν(C-COO) + δ(in-plane ring)
	845		δ(COO) + δ(in-plane ring) (6b)
		843	ν(C-COO) + δ(OCO)
933	*934*	*932*	*ν_s(Cl-O) from ClO_4^- ions*
1011	1002	1010	ν_{12} (trigonal ring breathing)
1038			β(CH) + ν(CC) + β(NH)
	1050	1049	β(CH)
1389	1390		ν_s(COO) + β(CH) + β(NH)
		1380	ν_s(COO) + β(CH)
	1437	1435	ν(CC, CN) (19b) + β(CH)
	1475	1470	ν(CC, CN) (19a) + β(CH)
		1575	*G mode from HOPG*
1621			ν(CC) (8a)

Key: β = in-plane bending, ν = stretching, and δ = in-plane deformation modes.
[a] Denoted using Wilson notation [20].

potentiodynamic silver deposition onto HOPG electrodes in presence of PA, at pH 3.0. Fig. 3 shows a comparison between the normal Raman spectra of PA solutions at pH 3.0 (I) and 6.5 (II) and the SERS spectrum of adsorbed PA molecules on silver crystallites growing at -0.45 V in pH 3.0 solution (III). Table 2 includes the assignments for the PA principal vibrational bands obtained from bibliography and DFT calculations [14,18,19].

The main differences between the normal Raman spectra of PA solutions at pH 3.0 and 6.5 are the shifting of the **838** and **1038** cm^{-1} bands towards higher energies for the solution with **Pic**$^-$ anion as predominant species, and the presence of new bands at **1437** and **1475** cm^{-1}, due to deprotonation of the pyridinic ring. Fig. 3 also clearly shows that, despite the predominant PA species in solution being **HPic**, the SERS spectrum (III) corresponds to **Pic**$^-$ adsorbed on the silver surface. The only difference between **Pic**$^-$ solution and SERS spectra lies in the wavenumber change for the trigonal ring breathing mode from **1002** to **1010** cm^{-1}, which in the SERS spectrum is due to direct **Pic**$^-$ interaction via N pyridinic ring. Since this is the most intense signal in SERS spectra, it is possible to assert that the additive molecules are perpendicularly adsorbed on the silver surface. Furthermore, the strong intensities of the -COO$^-$ group signals at **1380** and **843** cm^{-1}, indicate that the **Pic**$^-$ species also interacts with the silver surface via the carboxylate group. In summary, these results provide evidence that the additive molecules are perpendicularly adsorbed on the silver surface via both functional groups: N-pyridine ring and –COO$^-$ [14].

Fig. 4 contains SERS intensity results for the main vibrational bands of PA species and ClO_4^- ions at the electrode/electrolyte interface, during the potentiodynamic silver deposition and dissolution processes shown in Fig. 1. The top section of Fig. 4(a and b), includes the cathodic (blue) and anodic (red) j/E profiles in the range between +0.4 V and -0.9 V, whilst the corresponding SERS signals are shown in the bottom section of this figure.

Changes in the perchlorate ions signals at **931** cm^{-1} are clearly shown to occur during both cathodic and anodic potential scans, and are directly correlated with the changes observed in the intensity of the PA bands, which implies a co-adsorption effect of ClO_4^- ions. In contrast, and as a consequence of SERS selection rules, the dependence of SERS intensity on the potential during the voltammetric experiment is different for each PA vibrational mode [20,21]. It is well known that the intensity increase in the signals of vibrational modes with perpendicular components to the surface, or with the functional groups interacting directly with the silver surface [22], is dependent on the molecular adsorption geometry. In the present case, the intensity enhancement of bands at **1380** and **1014** cm^{-1}, corresponding to -COO$^-$ group stretching and pyridinic ring breathing, implies that **Pic**$^-$ is adsorbed with the pyridinic ring perpendicular to the silver surface and interacts via both functional groups: N pyridinic ring and -COO$^-$, as already pointed out [14].

In Fig. 4a, the SERS intensity of all bands increases simultaneously with silver deposition, which begins at around –0.2 V. However, when the potential approaches -0.65 V, the absolute intensity of all bands diminishes even though, at these cathodic potentials, growth of the Ag deposit continues on the HOPG surface. By reversing the potential scan at -0.9 V (Fig. 4b), the intensity increases again and reaches the maximum SERS scattering values at -0.1 V, when the amount of deposited silver is also a maximum. After this point, the SERS intensity diminishes due to silver dissolution. However, at potentials higher than +0.2 V,

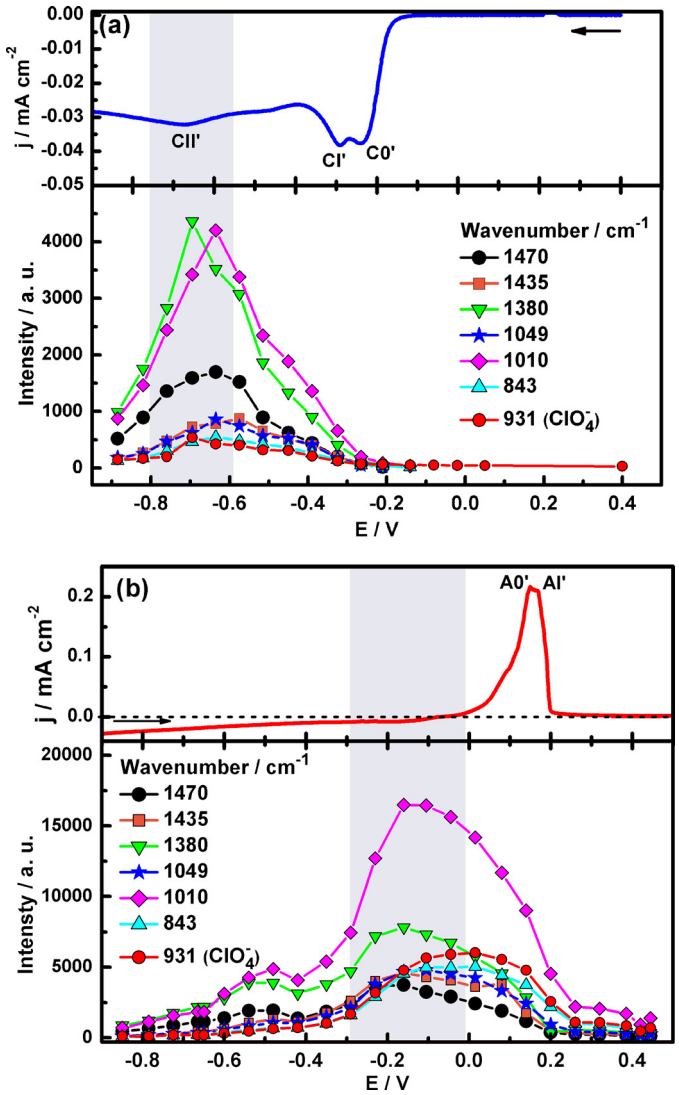

Fig. 4. Absolute SERS intensities of vibrational bands of PA (**843**,**1010**, **1049**, **1380**, **1435** and **1470** cm^{-1}) and ClO_4^- (**931** cm^{-1}) as a function of the applied potential during in-situ silver deposition and dissolution onto HOPG in 0.1 M $KClO_4$ + 1.0 mM $AgClO_4$ + 0.5 mM PA at pH 3.0. Potentiodynamic j/E profiles from **(a)** +0.4 V to -0.9 V (blue) and **(b)** -0.9 to +0.4 V (red). Scan rate: 1 mV s^{-1}. (For interpretation of the references to colour in this figure legend, the reader is referred to the web version of this article.)

an enhancement of the **Pic**$^-$ bands continues to be significant, thereby implying that silver dissolution is not complete and that SERS-active silver clusters remain on the HOPG surface.

The decrease in Raman intensity observed in the potential range between -0.6 V and -0.9 V in Fig. 4a can be caused by: i) desorption of the PA molecules; ii) occurrence of faradaic reactions involving additive molecules or iii) change in the size and morphology of the crystallite deposits (with lower activity for SERS). Since the changes in the geometry of the adsorbed molecules on the surface (bidimensional phase transition) and the electroreduction of the molecules to yield aldehydes and alcohol derivatives, which occurs at more negative potentials on a silver electrode, may be discarded as no new Raman bands are observed [23,24], only the first cause is considered in Section 3.3.

3.3. C-E curves of PA adsorption onto HOPG and Ag-HOPG electrodes

In order to establish the potential range for adsorption/desorption of PA molecules onto HOPG and HOPG with deposited silver crystallites, differential capacity curves at different potentials were recorded. Changes in the double layer capacity are very sensitive to the presence of adsorbates in the interfacial environment (electrolyte solution/electrode surface) [9,25,26]. Electrochemical impedance spectroscopy measurements of the HOPG electrode in both absence and presence of PA were required to determine the frequency at which the system displays a predominantly capacitive response in the potential range of interest. The optimal frequency value is 20 Hz and the corresponding electrochemical impedance spectra are shown in Fig. S1 of the Supporting Information. Differential capacity-potential (C-E) curves of HOPG electrodes in 0.1 M $KClO_4$ solution at pH 3.0 are shown in Fig. 5a (data correspond to both cathodic and anodic potential scans obtained with different HOPG electrodes).

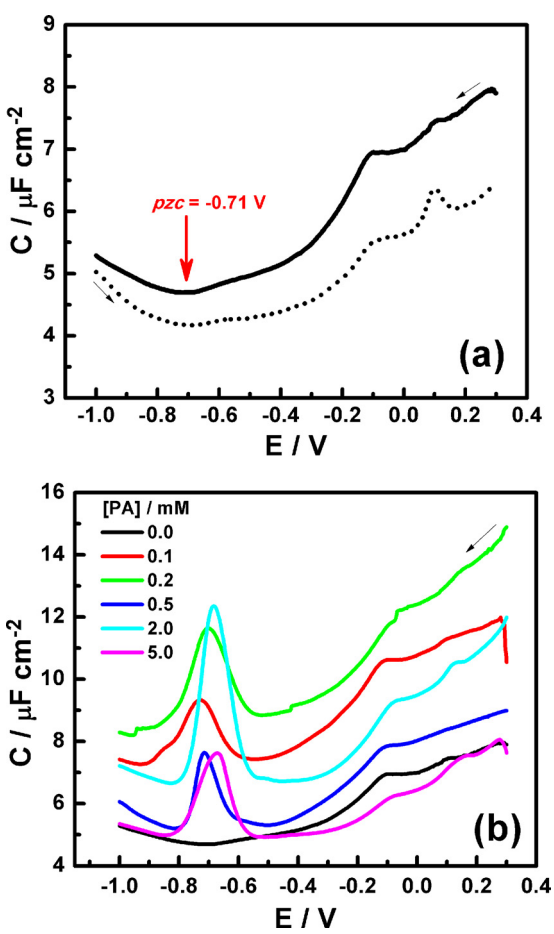

Fig. 5. C-E curves for HOPG in **(a)** 0.1 M $KClO_4$ at pH 3.0 (solid line for cathodic direction and dashed line for anodic potential scan); pzc = -0.71 V; **(b)** 0.1 M $KClO_4$ + ***x*** mM PA at pH 3.0 (***x*** = 0, 0.1, 0.2, 0.5, 2.0 and 5.0) during the cathodic scan. Frequency: 20 Hz. Scan rate: 10 mV s^{-1}.

The value of -0.71 V for the zero charge potential (pzc) of the HOPG surface was determined from the minimum in the C-E plot of Fig. 5a. The surface is positively charged at potentials higher than the pzc, but negatively charged at lower potentials. Values of pzc = -0.55 V for HOPG in 0.05 M HCl solution, have been reported in the literature [27], and some authors have shown that the differential capacity for HOPG depends on the electrolyte composition, pH and the potential range [28,29]. In Fig. 5a, the electrochemical sensitivity of these methods for the detection of surface defects can be appreciated since, although the C-E shape is the same, the curves correspond to different surfaces (after exfoliation of the outer layer), and therefore have different surface capacity values.

In the presence of PA at pH 3.0 (Fig. 5b), double layer capacity values for HOPG electrodes are higher than in the additive-free electrolyte, in contrast to the behavior observed for adsorption of organic compounds on metal surfaces [30]. No dependence of the capacity on the PA concentration in solution is observed, probably because of a different number of surface defects present in each HOPG surface. In addition, a capacity maximum at around -0.7 V, which is the value of HOPG-pzc in the supporting electrolyte, is observed. The j/E profiles of the electrode in the electrolyte with several PA concentrations and different pH (See Fig. S2 in Supporting Information) clearly show current maxima at -0.75 V that increase with decreasing solution pH and increasing PA concentration. In consequence, the cathodic current peak **CII'** found at pH 3.0 is assigned to the H^+ ions reduction reaction, coming from the acid dissociation of PA zwitterion species, according to the following reaction sequence, (5) and (6):

$$HPic \rightleftarrows Pic^- + H^+ \quad (5)$$

$$H^+ + e^- \rightarrow \tfrac{1}{2}H_2 \quad (6)$$

The faradaic current density at -0.7 V produces an increase in the double layer capacity as evidenced by the fact that the system electric response cannot be fitted to the RC equivalent circuit necessary to consider the interfacial charge transfer. Therefore, reported capacity values in the potential range between -0.6 and -0.8 V are not accurate. Moreover, when C-E profiles include a capacity maximum related to an adsorption/desorption process (without the faradaic process), the C-E curves should be coincident with those recorded in absence of PA (or at least show lower capacity) at more negative potentials. Thus, the magnitude of the capacity maximum should depend on PA concentration, a result that was not observed. In summary, the current maximum at -0.7 V is associated with the reaction mechanism described by (5) and (6), that is, molecular hydrogen formation from the acid equilibrium of **HPic** that leads to mechanical **Pic**$^-$ desorption. This observation is similar to that reported by Portela et al. for copper deposition onto Pt electrodes in the presence of PA [31]. Since vibrational signals in the in-situ SERS spectra during silver electrodeposition are only derived from the PA molecules adsorbed on silver crystallites (although the PA adsorption occurs onto both HOPG and silver surfaces), we have performed capacity measurements at different potentials with HOPG electrodes containing deposited silver crystallites. In this case, silver was

potentiodinamically deposited onto HOPG in 0.1 M $KClO_4$ + 1.0 mM $AgClO_4$ solutions at pH 3.0, the potential was scanned from +0.4 V to -0.5 V and reversed back to -0.1 V at 20 mV s^{-1}. Subsequently, the electrode was rinsed with Milli Q water and transferred to another electrochemical cell containing ***x*** mM PA (***x*** = 0.0, 0.5, 1.0 or 5.0) + 0.1 M $KClO_4$ at pH 3.0, with which the electrochemical impedance measurements were recorded (See Fig. S3 in the Supporting Information).

Fig. 6 shows the C-E curves obtained when the PA content in solution is modified. The experiments were carried out during the anodic potential scan, in order to avoid the electrochemical dissolution of Ag deposit at the beginning of the experiment. By comparing the results obtained with both substrates in absence of PA (Figs. 5 and 6), a value of -0.89 V for the pzc of Ag-HOPG electrode (more negative than for a clean HOPG surface) is established. Since Van Krieken et al. [32] have reported a pzc for Ag (111) of -1.02 V (vs. Ag/Ag^+ in 0.1 M $KClO_4$), the pzc obtained from C-E curves in Fig. 6 appears to correspond to a "mixed" surface.

All C-E curves in Fig. 6 have a maximum at +0.03 V, which is associated with silver deposit dissolution. Moreover, in contrast to the results in Fig. 5, there is a systematic change in the capacity values with additive concentration in solution, probably because the silver deposit (initially generated at the step edges of HOPG) produces a more reproducible electrode surface, independent of HOPG defects. When PA adsorption is studied during silver deposition (Fig. 5b), no correlating trend is found between the magnitude of the capacity maximum at -0.7 V and the additive content in the solution. In addition, the differential capacity at more negative potentials does not reach the observed values for HOPG in the absence of PA, which indicates absence of an electrochemical adsorption/desorption process onto the silver crystallites. However, the capacity maximum cannot be assigned to a 2D-phase transition because, in SERS spectra at potentials more negative than -0.7 V, new vibrational signals or changes in the relative intensities are not detected [33,34]. Furthermore, the maximum at -0.74 V in the presence of PA, is associated with the electroreduction of protons produced by the acid dissociation equilibrium of PA zwitterion on the Ag-HOPG surface (Reactions (5) and (6)). Fig. 4a clearly shows that the **CII'** peak occurs at the potential at which Raman intensity is a maximum, and corresponds to the PA desorption maximum, as evidenced in the anodic C-E curves (Fig. 6). These results indicate that the decrease in Raman intensity at potentials more negative than -0.7 V is due to hydrogen formation from **HPic** in the solution bulk. In addition, molecular H_2 produced at the surface promotes mechanical PA desorption, thereby decreasing its surface concentration and, therefore, the SERS signals intensity.

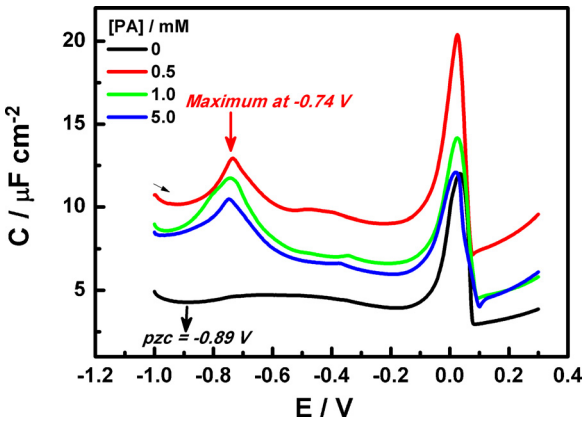

Fig. 6. C-E curves for Ag-HOPG electrodes in 0.1 M $KClO_4$ + ***x*** mM PA (***x*** = 0.0, 0.5, 1.0 and 5.0) at pH 3.0; pzc = -0.89 V. Only data of anodic potential scans are shown. Frequency: 20 Hz. Scan rate: 10 mV s^{-1}.

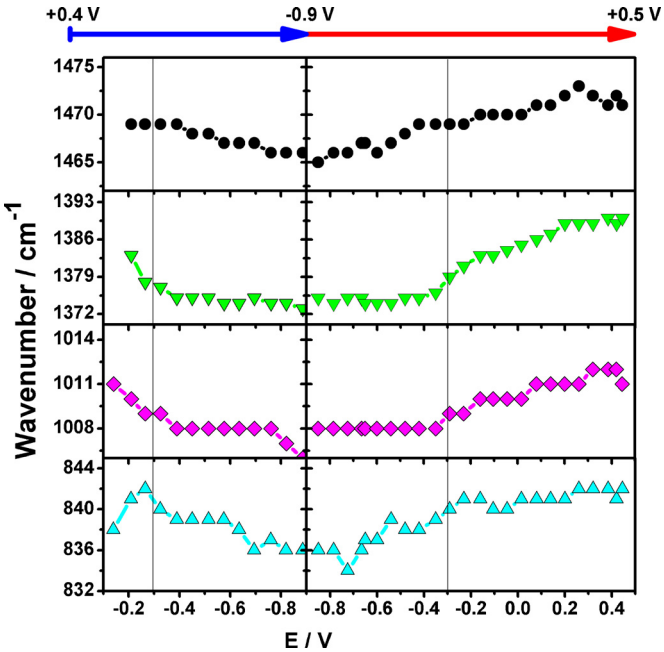

Fig. 7. Wavenumber vs. potential dependence for the main SERS PA signals at **1470**, **1380**, **1010** y **843** cm^{-1} during silver deposition and dissolution onto HOPG in 0.1 M $KClO_4$ + 1.0 mM $AgClO_4$ + 0.5 mM PA at pH 3.0. Potentiodynamic scans from +0.4 V to -0.9 V (left side, blue arrow) and -0.9 to +0.4 V (right side, red arrow). Scan rate: 1 mV s^{-1}. (For interpretation of the references to colour in this figure legend, the reader is referred to the web version of this article.)

3.4. Wavenumber-potential dependence during silver electrodeposition onto HOPG in the presence of PA

Fig. 7 shows the changes in the wavenumber of PA SERS signals at **1470** (ν(CC,CN) 19a + β(CH)), **1380** (β(CH) + ν_s(COO^-)), **1010** (ν(ring) 12) and **843** (δ(COO) + δ(ring) 6b) cm^{-1}, observed during both cathodic (blue arrow) and anodic (red arrow) potential scans. Assignments of vibrational bands are presented in Table 2.

The main PA bands wavenumber decreases as the applied potential becomes increasingly negative (blue arrow), whereas an increase in the wavenumber, back to the original value at the same potential, is observed during the anodic potential scan (red arrow). Consequently, since the position of the band at a given potential is the same irrespective of the scan direction, the frequency of each vibrational mode depends only on the electrode surface charge and its interaction with the adsorbed molecules. It is apparent that vibrational frequencies do not depend on the amount of silver deposit or the number of SERS sites on the surface. For example, since at -0.3 V the electrode surface is positively charged (pzc of HOPG-Ag = -0.89 V), the interaction with the adsorbed molecules is very strong (specifically with the picolinate anion, which has a net negative charge) and the frequency of the corresponding vibrational modes is blue-shifted (that is, the vibrational energy increases), feature that evidence the formation of highly coordinated bonds [35]. As the potential approaches the pzc value, weakening of the interactions involving **Pic**$^-$ species correlates with a decrease of both, the positive charge density on the surface and the frequency values. A similar situation occurs when the potential scan is reversed at -0.9 V, because the surface is becoming more positively charged and a stronger interaction with PA (increasing frequency) is promoted. On the contrary, at potentials more negative than pzc, PA desorption leads to a decrease in the

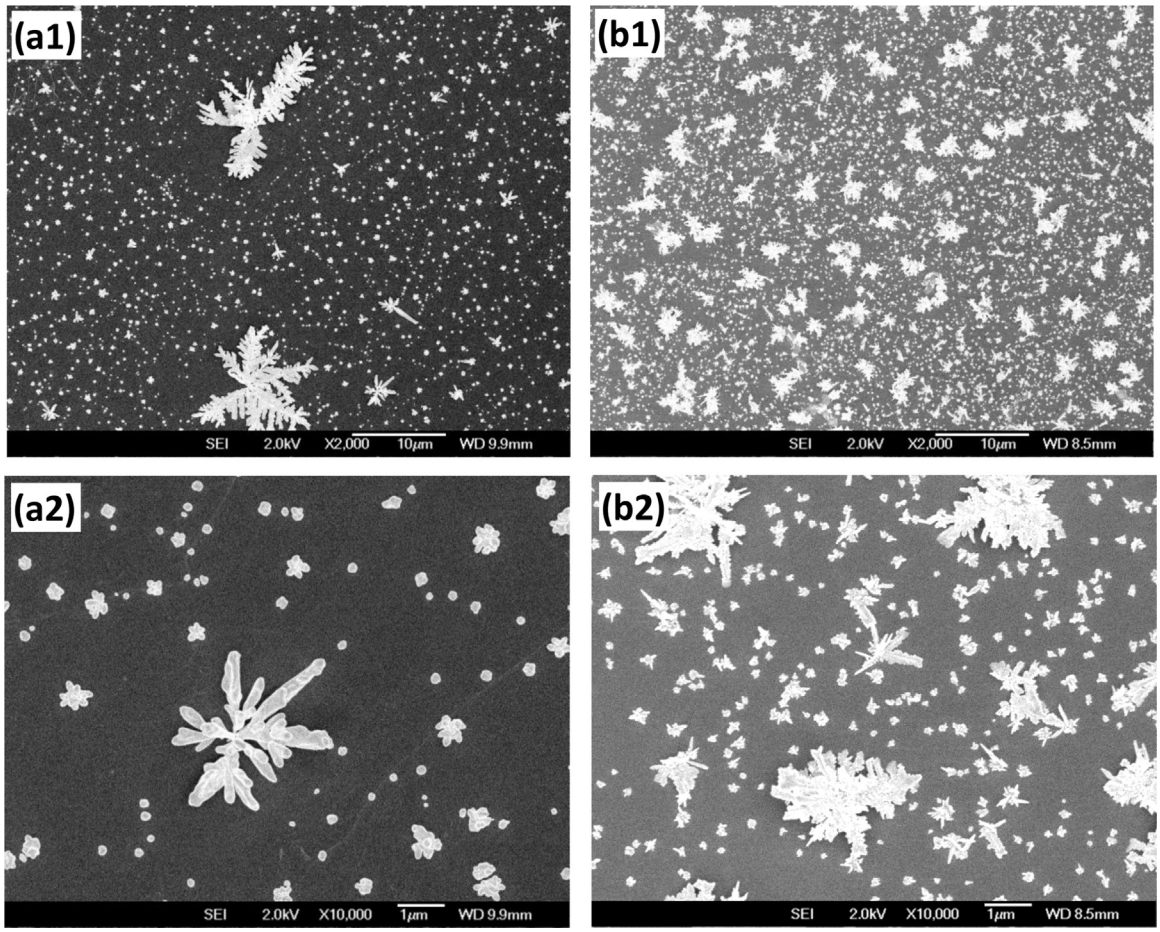

Fig. 8. SEM micrographs at two different magnifications of HOPG electrodes after silver deposition by potentiodynamic scan from +0.4 V to -0.9 V and returning to -0.1 V in 0.1 M $KClO_4$ + 1.0 mM $AgClO_4$ + **(a)** 0 mM PA or **(b)** 1.0 mM PA solutions at pH 3.0. Scan rate: 1 mV s^{-1}.

corresponding SERS intensity and, thus, PA molecules can only be detected in spectra recorded at potentials more positive than pzc.

These experiments are valuable to answering the following question: why is the **Pic**$^-$ anion the adsorbed species when the electrolyte pH is 3.0 and **HPic** is the predominant PA species? This phenomenon is the result of several factors. First, as the surface becomes positively charged (at potentials higher than pzc), the H^+ ions concentration becomes very low in the electrode/electrolyte interface relative to the solution bulk. Second, the ionic species (anion) has greater stability compared to the neutral species (zwitterion) due to "image charge" coulombic attraction, resulting in an effectively lower pKa value. Furthermore, the **Pic**$^-$ ligand in the **Ag^0-(Pic$^-$)** surface complex interacts with the silver surface via two sites (or functional groups): pyridinic N (covalent attraction) and -COO^- (coulombic attraction), whereas **HPic** interacts only via–COO^- [36]. In summary, **Pic**$^-$ is preferentially adsorbed onto the silver surface and **HPic** molecules easily lose their H^+ to became anionic species, resulting in acid-base equilibria on the electrode surface that are different from those in the solution bulk [20,37,38].

3.5. SEM characterization of silver deposits

The morphology of silver crystallites potentiodynamically deposited onto HOPG in both absence and presence of PA is displayed in Fig. 8. SEM micrographs of Ag deposits resulting from a cathodic potential scan up to -0.9 V and back to -0.1 V at 1 mV s^{-1} exhibit typical hierarchical dendritic patterns, with a non-homogeneous distribution of crystallites size (Fig. 8). It is generally accepted that dendritic formation occurs by a diffusion limited aggregated (DLA) growth model including nucleation, adsorption and branched growth processes [39]. During electrodeposition at low metal cation concentration (< 25 mM), shielding effects occur due to an inhomogeneous distribution of the metallic ions around the initial nuclei centers, with diffusion as rate limiting step. This effect becomes enhanced with time, resulting in the formation of dendritic-type microstructures [40,41].

In Figs. 8a1 and 8a2 corresponding to silver deposition in a free-additive solution, different types of morphologies and sizes for the crystallites, ranging from very large fern-like structures with branches of up to 10 μm in length to rounded small particles with sizes as large as 50 nm, are evidenced. In all cases, the structures are smooth with no sharp edges. In contrast, silver crystallites electrodeposited in the presence of PA (Fig. 8b) exhibit a flower-like structure with narrower and smaller branches, characterized by lengths of up to 2 μm. This kind of morphology results from a fast nucleation, followed by slow aggregation and crystallization, of primary particles [42]. Furthermore, the effect of PA on the growing phase becomes apparent in that the **Pic**$^-$ anion can be preferentially adsorbed on certain crystalline faces of the silver nuclei surface, thereby promoting different growth rates along these faces.

4. Conclusions

Adsorption of picolinic acid onto HOPG electrodes during silver potentiodynamic electrodeposition at pH 3.0 has been studied by

cyclic voltammetry, electrochemical impedance measurements, and in-situ SERS spectroscopy. Spectroscopic analysis of the potential dependence of absolute intensities of Raman bands from PA and the respective voltammetric results confirm that the **Pic**$^-$ anion is the species adsorbed on the growing silver crystallites, even though the **HPic** zwitterion is the predominant species in the electrolyte at pH 3.0. The **Pic**$^-$ anion is perpendicularly adsorbed and interacts with the silver surface via both functional groups: pyridinic N and –COO$^-$.

In-situ SERS has been shown to be able to reveal details of the interfacial chemistry relevant to a more insightful understanding of the electrodeposition process. A "step by step" tracking (potential by potential) of silver deposition onto and dissolution from HOPG, and the simultaneous adsorption of **Pic-**, can be effected by exploring correlations between in-situ SERS spectra, cyclic voltammetry, and differential capacity of the interface in 0.1 M $KClO_4$ + 1.0 mM $AgClO_4$ + 0.5 mM PA solution at pH 3.0:

- in the cathodic scan at +0.4 V, the potential is not sufficiently negative for silver ion electroreduction to occur, and in the SERS spectra, only the HOPG and ClO_4^- ions signals are detected. When the potential becomes more negative than -0.15 V, silver electrodeposition starts from reduction of free Ag^+ ions (**C0'** peak, at -0.24 V) and **[Ag(Pic)]** complexes (**CI'** peak, at -0.29 V) and, therefore, **Pic**$^-$ SERS signals are evidenced. The intensity of PA SERS signals increases with electrode potential due to the increasing amount of silver deposit and, consequently, the higher number of SERS active sites for PA molecules adsorption. However, this is accompanied by a decrease in PA bands frequency because the surface become less positively charged as the potential approaches the HOPG-pzc and the surface-adsorbate interaction becomes weaker. A decrease in the pKa of the additive at the electrode/electrolyte interface compared to solution bulk is evidenced because, in this potential range, the electrode surface is positively charged.

- at -0.7 V (HOPG-pzc; **CII'** peak) decrease of SERS intensity is directly correlated with increased differential capacity at the electrode/electrolyte interface, which originates from reduction of H^+ ions produced by the PA zwitterioṅs acid dissociation equilibrium, and results in desorption of additive molecules induced by $H_{2(g)}$ formation on the surface.
- in the anodic scan, the surface charge density becomes increasingly positive, leading to an enhancement of the substrate-adsorbate interaction and the bands frequency in the SERS spectra. The maximum PA SERS enhancement is found at -0.1 V, corresponding to a maximum in charge density for silver deposition, whilst the decrease in SERS signal intensity is caused by silver deposit dissolution (peaks **A0'** and **A0"**).

Silver electrodeposited crystallites in the presence of PA have a flower-like structure with narrower and smaller branches than in the free-additive electrolyte. These structures can be obtained as a result of preferential **Pic**$^-$ adsorption on certain crystalline faces of the silver nuclei surface, which promotes different growth rates along these faces.

Acknowledgments

This research has been supported with funds from CNPq, FAPESP, CONICET, FONCyT, SECyT-UNC, PME 1544 and Central Analitica-IQ-USP (FEG-SEM facilities). G.F.S.A. thanks FAPESP for fellowships, and M.L.A.T. thanks CNPq for the research fellowship.

Appendix A. Supplementary data

Supplementary data associated with this article can be found, in the online version, at http://dx.doi.org/10.1016/j.electacta.2015.01.034.

References

[1] M. Schlesinger, M. Paunovic, Modern Electroplating, John Wiley & Sons, Inc., 2011.
[2] T.M.T. Huynh, F. Weiss, N.T.M. Hai, W. Reckien, T. Bredow, A. Fluegel, et al., On the role of halides and thiols in additive-assisted copper electroplating, Electrochim. Acta. 89 (2013) 537–548.
[3] Z.-B. Lin, J.-H. Tian, B.-G. Xie, Y.-A. Tang, J.-J. Sun, G.-N. Chen, et al., Electrochemical and in Situ SERS Studies on the Adsorption of 2-Hydroxypyridine and Polyethyleneimine during Silver Electroplating, J. Phys. Chem. C. 113 (2009) 9224–9229.
[4] J. Ustarroz, X. Ke, A. Hubin, S. Bals, H. Terryn, New Insights into the Early Stages of Nanoparticle Electrodeposition, J. Phys. Chem. C. 116 (2012) 2322–2329.
[5] G. Staikov, A. Milchev, Electrocrystallization in Nanotechnology, Wiley-VCH Verlag, 2007.
[6] L.P. Bicelli, B. Bozzini, C. Mele, L. D'Urzo, A Review of Nanostructural Aspects of Metal Electrodeposition, Int. J. Electrochem. Sci. 3 (2008) 356–408.
[7] D. Gonnissen, A. Hubin, J. Vereecken, EIS combined with SERS: a tool to study the adsorption of S2O3(2-) and PMT in silver electroplating conditions, Electrochim. Acta. 44 (1999) 4129–4137.
[8] Y.-C. Pan, Y. Wen, X.-Y. Guo, P. Song, S. Shen, Y.-P. Du, et al., 2-Amino-5-(4-pyridinyl)-1,3,4-thiadiazole monolayers on copper surface: Observation of the relationship between its corrosion inhibition and adsorption structure, Corros. Sci. 73 (2013) 274–280.
[9] A. Hubin, D. Gonnissen, W. Simons, J. Vereecken, Spectro-electrochemical study of the influence of ligand adsorption on the reaction rate of the electrodeposition of silver complexes, J. Electroanal. Chem. 600 (2007) 142–150.
[10] A.L. Portela, M. López Teijelo, G.I. Lacconi, Mechanism of copper electrodeposition in the presence of picolinic acid, Electrochim. Acta. 51 (2006) 3261–3268.
[11] J. Barthelmes, W. Plieth, SERS investigations on the adsorption of pyridine carboxylic acids on silver- Influence of pH and suporting eletrolyte, Electrochim. Acta. 40 (1995) 2487–2490.
[12] A.E. Bolzán, Electrodeposition of copper on glassy carbon electrodes in the presence of picolinic acid, Electrochim. Acta. 113 (2013) 706–718.
[13] C.I. Vázquez, G.I. Lacconi, Nucleation and growth of silver nanostructures onto HOPG electrodes in the presence of picolinic acid, J. Electroanal. Chem. 691 (2013) 42–50.
[14] C.I. Vázquez, G.F.S. Andrade, M.L.A. Temperini, G.I. Lacconi, Monitoring of Silver Electrodeposition onto HOPG Electrodes in the Presence of Picolinic Acid by in Situ Surface-Enhanced Raman Spectra Measurements, J. Phys. Chem. C. 118 (2014) 4167–4180.
[15] K.H. Ng, H. Liu, R.M. Penner, Subnanometer Silver Clusters Exhibiting Unexpected Electrochemical Metastability on Graphite, Langmuir. 16 (2000) 4016–4023.
[16] R.T. Pötzschke, C.A. Gervasi, S. Vinzelberg, G. Staikov, W.J. Lorenz, Nanoscale studies of Ag electrodeposition on HOPG (0001), Electrochim. Acta. 40 (1995) 1469–1474.
[17] S. Kotrlý, L. Šůcha, Handbook of Chemical Equilibria in Analytical Chemistry, Ellis Horwood Limited, Chichester, England, 1985.
[18] Y. Liang, L.K. Noda, O. Sala, Polarizability and concentration effects on the Raman spectra of picolinic acid species in aqueous solution, J. Mol. Struct. 554 (2000) 271–277.
[19] L.-R. Wang, Y. Fang, UV-Raman study and theoretical analogue of picolinic acid in aqueous solution, J. Mol. Spectrosc. 234 (2005) 137–142.
[20] M. Moskovits, J.S. Suh, The geometry of several molecular ions adsorbed on the surface of colloidal silver, J. Phys. Chem. 88 (1984) 1293–1298.
[21] M. Moskovits, J.S. Suh, Surface Selection Rules for Surface-Enhanced Raman Spectroscopy: Calculations and Application to the Surface-Enhanced Raman Spectrum of Phthalazine on Silver, J. Phys. Chem. 88 (1984) 5526–5530.
[22] R.L. McCreery, Raman Spectroscopy for Chemical Analysis, John Wiley & Sons Inc., 2000.
[23] M. Ud Din Bhatti, O.R. Brown, Reductions of pyridine monocarboxylic acids and carboxaldehydes at mercury cathodes, J. Electroanal. Chem. 68 (1976) 85–95.
[24] K.A. Bunding, M.I. Bell, Surface-enhaced Raman spectroscopy of pyridine derivatives: effects of adsorption on electronic structure, Surf. Sci. 118 (1983) 329–344.
[25] J.V. Zoval, P.R. Biernacki, R.M. Penner, Implementation of Electrochemically Synthesized Silver Nanocrystallites for the Preferential SERS Enhancement of Defect Modes on Thermally Etched Graphite Surfaces, Anal. Chem. 68 (1996) 1585–1592.
[26] A.J. Bard, L.R. Faulkner - Electrochemical Methods, Fundamentals and Applications, Wiley New York, 1980. 1980 1980–1980.
[27] R.M. Nyffenegger, R.M. Penner, Nanometer-Scale Electropolymerization of Aniline Using the Scanning Tunneling Microscope, J. Phys. Chem. 100 (1996) 17041–17049.

[28] J.-P. Randin, E. Yeager, Differential capacitance study on the edge orientation of pyrolytic graphite and glassy carbon electrodes, J. Electroanal. Chem. Interfacial Electrochem. 58 (1975) 313–322.
[29] E.J. Bottani, J.M.D. Tascón, eds., Adsorption by Carbons, Elsevier, 2008.
[30] A. Łukomska, J. Sobkowski, Adsorption of thiourea on monocrystalline silver electrodes in neutral solution, Electrochim. Acta. 51 (2006) 2247–2254.
[31] A.L. Portela, PhD thesis: Influence of additives in metal plating processes, National University of Córdoba, 2004.
[32] M. Van Krieken, C. Buess-Herman, On the adsorption of uridine at the Ag (111)/aqueous solution interface, Electrochim. Acta. 45 (1999) 675–683.
[33] W.-B. Cai, L. Wan, H. Noda, Y. Hibino, K. Ataka, M. Osawa, Orientational Phase Transition in a Pyridine Adlayer on Gold(111) in Aqueous Solution Studied by in Situ Infrared Spectroscopy and Scanning Tunneling Microscopy, Langmuir. 14 (1998) 6992–6998.
[34] J. Lipkowski, P.N. Ross, eds., Adsorption of Molecules at Metal Electrodes, VCH, Weinheim 1992.
[35] D.H.H. Dressler, Y. Mastai, M. Rosenbluh, Y. Fleger, Surface-enhanced Raman spectroscopy as a probe for orientation of pyridine compounds on colloidal surfaces, J. Mol. Struct. 935 (2009) 92–96.
[36] J. Barthelmes, W. Plieth, SERS investigation on the adsorption of pyridine carboxylic acids on silver - Influence of pH and supporting electrolite, Electrochim. Acta. 40 (1995) 2487–2490.
[37] J.S. Suh, M. Moskovits, Surface-enhanced Raman spectroscopy of amino acids and nucleotide bases adsorbed on silver, J. Am. Chem. Soc. 108 (1986) 4711–4718.
[38] L.K. Noda, O. Sala, SERS effect of isonicotinic acid adsorbed on a copper electrode, J. Mol. Struct. 162 (1987) 11–17.
[39] T.A. Witten, L.M. Sander, Diffusion-Limited Aggregation, a Kinetic Critical Phenomenon, Phys. Rev. 47 (1981) 1400–1403.
[40] R. Sivasubramanian, M.V. Sangaranarayanan, Electrodeposition of silver nanostructures: from polygons to dendrites, CrystEngComm. 15 (2013) 2052.
[41] D.K. Sharma, A. Ott, A.P. O'Mullane, S.K. Bhargava, The facile formation of silver dendritic structures in the absence of surfactants and their electrochemical and SERS properties, Colloids Surfaces A Physicochem. Eng. Asp. 386 (2011) 98–106.
[42] S. Zeng, K. Tang, T. Li, Z. Liang, 3D flower-like Y(2)O(3):Eu(3+) nanostructures: template-free synthesis and its luminescence properties, J.Colloid Interface Sci. 316 (2007) 921–929.